Physica D 241 (2012) 137–140

Contents lists available at SciVerse ScienceDirect

Physica D

journal homepage: www.elsevier.com/locate/physd

The ultimate state of thermal convection in Rayleigh–Taylor turbulence

G. Boffetta [a,b,*], F. De Lillo [a], A. Mazzino [c], L. Vozella [c]

[a] Dip. di Fisica Generale and INFN, via P.Giuria 1, 10125 Torino, Italy

[b] CNR-ISAC, Sezione di Torino, corso Fiume 4, 10133 Torino, Italy

[c] Dip. di Fisica, INFN and CNISM, Università di Genova, via Dodecaneso 33, 16146 Genova, Italy

ARTICLE INFO

Article history:
Available online 9 November 2011

Keywords:
Turbulence
Mixing
Thermal convection

ABSTRACT

This paper discusses the so-called *ultimate state* of thermal convection, first proposed by Kraichnan almost 50 years ago and recently observed in numerical simulations of turbulent convection in the absence of boundaries. We focus on numerical simulations of turbulence generated by the Rayleigh–Taylor instability in a wide range of Rayleigh and Prandtl numbers. Our results point out to the conclusion that RT turbulence provides a natural realization of the ultimate state of thermal convection thus highlighting the relationship between the absence of boundaries and the emergence of the *ultimate state* scaling for global statistical quantities.

1. Introduction

Turbulent thermal convection is one of the most important manifestations of turbulence as it appears in many natural phenomena, from heat transport in stars [1] to atmospheric [2,3] and oceanic mixing [4,5]. Turbulent convection also plays a fundamental role in many technological applications where it is an efficient mechanism for exchanging heat [6]. When turbulent convection arises as a consequence of the gravitational instability at the interface of two layers of fluid at different temperatures one has the case of Rayleigh–Taylor (RT) turbulence which finds specific applications in geophysics (e.g. in cloud formation [7]), astrophysics (thermonuclear reactions in type-Ia supernovae [8]) and in inertial confinement fusion [9].

RT turbulence arises as a transient state in which initial potential energy is gradually converted into turbulent kinetic energy. Turbulence enhances the mixing of the temperature field, making the transfer of heat much more efficient than in the non-turbulent case. A quantitative measure of this efficiency is given by the Nusselt number Nu, the ratio of the global turbulent heat transfer to the molecular one, while a natural measure of turbulent intensity is provided by the Reynolds number Re. These two numbers represent the status of the turbulent flow while the control parameters are the Rayleigh number Ra (a dimensionless measure of the temperature difference between the two layers) and the Prandtl number Pr (the ratio between kinematic viscosity ν and thermal diffusivity κ).

A natural problem in thermal convection is the characterization of the state of the system at given value of control parameters, i.e. the functional relation $Nu(Ra, Pr)$ and $Re(Ra, Pr)$. Many experimental investigations [10,11] together with numerical simulations [12] and theoretical arguments [13,14] suggest that, for well developed turbulent convection ($Ra \gg 1$) simple power laws hold

$$Nu \sim Ra^{\gamma} Pr^{\delta} \qquad Re \sim Ra^{\alpha} Pr^{\sigma} . \tag{1}$$

Within this framework, Kraichnan [15] predicted an asymptotic regime, now called *ultimate state*, for which the exponents assume the values [16,13] $\alpha = \gamma = \delta = 1/2, \sigma = -1/2$. The ultimate state regime is expected to hold in general at very large Ra when thermal and viscous boundary layers (if present) break down and convection is dominated by bulk contributions. In spite of big experimental efforts, the ultimate regime remains elusive in experiments of Rayleigh–Bénard turbulent convection where boundary layers play an important role [14]. Recent experiments done in vertical channels in absence of plates have shown indeed the appearance of a regime compatible with the ultimate state [17,18].

From the above considerations, it is natural to expect that the ultimate state regime governs thermal convection in RT turbulence because of the irrelevance of boundaries in this configuration. Indeed, recent numerical simulations of RT turbulence both in 2D [19] and 3D [20,21] at fixed $Pr = 1$ show the appearance of the $Ra^{1/2}$ dependence for both Nu and Re. We remark that the Kraichnan regime has also been observed in numerical simulations of turbulent convection in a periodic box forced by an unstable mean temperature gradient [22,23]. Within this framework we can consider RT setup as an adiabatically evolving turbulent flow which at each time realized a given set of parameters.

* Corresponding author at: Dip. di Fisica Generale and INFN, via P.Giuria 1, 10125 Torino, Italy. Tel.: +39 011 630 6813.
E-mail address: boffetta@to.infn.it (G. Boffetta).

0167-2789/$ – see front matter © 2011 Elsevier B.V. All rights reserved.
doi:10.1016/j.physd.2011.10.009

In the present paper, we investigate in details the ultimate state regime in RT turbulence on the basis of direct numerical simulations both in 2D and 3D in a wide range of control parameters Ra and Pr.

2. The model and the derivation of the ultimate state regime

We will consider Rayleigh–Taylor turbulence induced by two layers of fluid with small density difference. In this case the Boussinesq approximation for an incompressible fluid holds:

$$\partial_t \mathbf{v} + \mathbf{v}\cdot\nabla\mathbf{v} = -\frac{1}{\rho}\nabla p + \nu\nabla^2\mathbf{v} - \beta\mathbf{g}T, \tag{2}$$

$$\partial_t T + \mathbf{v}\cdot\nabla T = \kappa\nabla^2 T. \tag{3}$$

In (2)–(3) $\mathbf{v}(\mathbf{x}, t)$ is the incompressible ($\nabla\cdot\mathbf{v} = 0$) velocity field, $T(\mathbf{x}, t)$ represents temperature fluctuations (with respect to a reference temperature $T = 0$), p is the pressure, ρ the (constant) density, $\mathbf{g} = (0, 0, -g)$ the gravitational acceleration and β the thermal expansion coefficient.

The initial condition (at $t = 0$) is a layer of cooler (heavier) fluid on the top of a hotter (lighter) layer at rest, i.e. $\mathbf{v}(\mathbf{x}, 0) = 0$ and $T(\mathbf{x}, 0) = -(\theta_0/2)\mathrm{sgn}(z)$ where θ_0 is the initial temperature jump which fixes the Atwood number $A = (1/2)\beta\theta_0$. As a consequence of the linear instability phase, the system develops a turbulent mixing zone which grows in time starting from the interface plane $z = 0$ [24]. The amplitude of root mean square velocity fluctuations within the mixing layer can be estimated by dimensional balance of the first (acceleration) and the last (buoyancy) terms in (2) as $u(t) \sim Agt$, which is nothing but growth under constant acceleration. As a consequence, the width of the mixing layer $h(t)$ grows according to $h(t) = \alpha A g t^2$ where α is a dimensionless parameter whose value (which of course depends on the precise definition of h) has been measured in different numerical simulations [8,21]. Several numerical simulations have shown that the mean temperature profile $\bar{T}(z)$ in the turbulent mixing layer closely follows a linear behavior, i.e. $\bar{T}(z) = -\gamma z$ with $\gamma(t) = \theta_0/h(t)$ [19–21,25].

Turbulent kinetic energy in the mixing layer $E = (1/2)\langle v^2\rangle$ is produced at the expense of potential energy $P = -\beta g\langle zT\rangle$ (brackets represent integral over the physical domain). From (2) the energy balance reads

$$\frac{dP}{dt} = \beta g\langle wT\rangle = \frac{dE}{dt} + \varepsilon_\nu, \tag{4}$$

where $\varepsilon_\nu = \nu\langle(\nabla\mathbf{v})^2\rangle$ is the viscous energy dissipation. Note that in writing (4) we have not taken into account the contribution of thermal diffusivity to the variation of potential energy (which in negligible in the turbulent case). Introducing the dimensionless global heat transfer $Nu \equiv (\langle wT\rangle h)/(\kappa\theta_0)$, (4) can be rewritten as

$$\kappa\frac{\beta g\theta_0}{h}Nu = \frac{d}{dt}\frac{1}{2}\langle u^2\rangle + \varepsilon_\nu. \tag{5}$$

Assuming that all the terms in (5) scale in the same way, using the dimensional behavior for $h(t)$ and $u(t)$, one obtains $Nu \sim (\beta g\theta_0)^2 t^3/\kappa$. From the definition of $Ra \equiv \beta g\theta_0 h^3/(\nu\kappa)$, one has $Ra \sim (\beta g\theta_0)^4 t^6/(\nu\kappa)$ and therefore the prediction [13]

$$Nu \sim Ra^{1/2}Pr^{1/2}. \tag{6}$$

Similarly, introducing the Reynolds number $Re \equiv uh/\nu \sim (\beta g\theta_0)^2 t^3/\nu$, one has

$$Re \sim Ra^{1/2}Pr^{-1/2}. \tag{7}$$

Relations (6)–(7) constitute the so-called ultimate state regime of Rayleigh–Taylor turbulence. We remark that this regime has been originally derived for bounded turbulent convection in the Rayleigh–Bénard configuration [15,13]. In that case it is expected to hold at very large Ra, when both viscous and thermal boundary layers give a negligible contribution to the heat transfer. From these considerations, it is not surprising that the ultimate state arises naturally in RT turbulence where boundaries play no role and convection is ruled by bulk properties of the mixing region. We also remark that the energy balance argument leading to (6)–(7) holds both in two and three dimensions, therefore the ultimate state regime is expected also in 2D turbulence despite the fact that in this case the energy flows to large scales (and hence $\varepsilon_\nu = 0$) with a spectrum different from the 3D case [19].

3. Results from direct numerical simulations

Ultimate range scaling (6)–(7) has been checked in direct numerical simulations of RT turbulence in both two and three dimensions. To this aim, we integrated the equation of motion (2)–(3) by means of a pseudo-spectral method (in both two-dimensional and three-dimensional versions) with MPI parallel implementation and a second-order Runge–Kutta time stepping. Typical resolution for the runs is $512\times512\times1024$ for 3D and 512×2048 for the 2D cases with cubic (square) lattices. Physical parameters are $\beta g = 0.5$ and $\theta_0 = 1$ for the 3D case and $\beta g = 0.25$ and $\theta_0 = 0.6$ for the 2D one.

The initial RT instability is triggered by adding a small disturbance at the interface. Specifically, we add a 10% of white noise to the value of $T(\mathbf{x}, 0)$ in a small layer of width h_0 around $z = 0$. The initial disturbance affects the initial development of the mixing layer, the velocity with which the turbulent stage is reached and the numerical coefficients. On the other hand, numerical coefficients are also clearly affected by the definition chosen for the mixing layer width $h(t)$. Several definitions have been proposed based on either local or global properties of the mean temperature profile. Here we define $h(t)$ using a threshold on the average temperature profile, i.e. $\bar{T}(z = \pm h) = \mp 0.8\frac{\theta_0}{2}$. Other values of the threshold can be used, e.g. 0.9 or 0.99, again only changing the values of numerical prefactors.

Each run provides a time evolution of the dimensionless numbers Ra, Re and Nu at fixed Pr, which has been chosen in a range of more than two decades $0.2 \le Pr \le 50$. We remark that from a numerical point of view, the most convenient condition is $Pr = 1$ for which ν and κ are both chosen as small as possible to have a large turbulent-convective range. Both $Pr \ll 1$ and $Pr \gg 1$ are numerically inefficient as one of the cascades is resolved with a large dissipative range. This is the main limitation to the available range of Pr.

The relevant statistics refers to the dynamics appearing after a fully turbulent mixing layer develops and before finite size effects due to vertical confinement and lateral periodicity become evident.

3.1. 3D configuration

Figs. 1 and 2 show the results of the three-dimensional simulations for Nu and Re, respectively, as a function of Ra and Pr. Data are obtained from a single realization for each Pr in which Ra evolves in time as discussed in Section 2.

The main plot in Fig. 1 shows that numerical data are compatible with (6) for $Ra > 10^7$, although fluctuations are observed, in particular at high Pr. The lower inset reports the Pr dependence at fixed $Ra = 3\times10^8$ where the $Pr^{1/2}$ scaling is observed.

In Fig. 2 we report the same data for the Reynolds number. At variance with Nu, here the rescaling with the $Pr^{-1/2}$ prediction of (7) suggests systematic deviations. Indeed the inset of Fig. 2 shows that the best fit exponent (-0.54) deviates from the

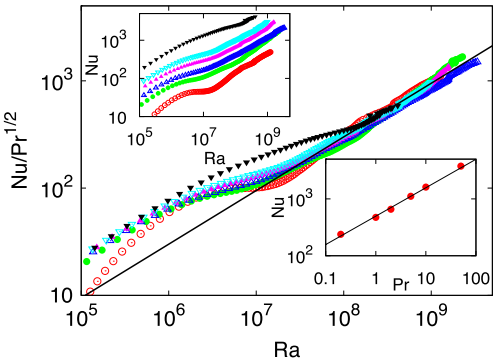

Fig. 1. *Nu* vs *Ra* obtained from 3D simulations at Prandtl numbers $Pr = 0.2$ (red, open circles), $Pr = 1.0$ (green, closed circles), $Pr = 2.0$ (blue, open upper triangles), $Pr = 5.0$ (pink, closed upper triangles), $Pr = 10.0$ (cyan, open lower triangles) and $Pr = 50$ (black, closed lower triangles) (upper inset). Each set of points at a given *Pr* are obtained from a single simulation of Eqs. (2)–(3) in which *Nu*, *Re* and *Ra* increase with time. Main plot: *Nu* compensated with ultimate state prediction $Pr^{1/2}$ vs *Ra*. The line represent $Ra^{1/2}$. Lower inset: *Nu* vs *Pr* at fixed $Ra = 3 \times 10^8$. The line represents the best fit with a slope 0.51 ± 0.02.

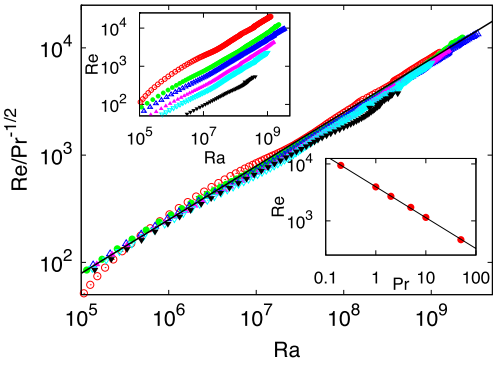

Fig. 2. *Re* vs *Ra* obtained from 3D simulations at different Prandtl numbers (colors and styles as in Fig. 1) (upper inset). Main plot: *Re* compensated with ultimate state prediction $Pr^{1/2}$ vs *Ra*. The line represent $Ra^{1/2}$. Lower inset: *Re* vs *Pr* at fixed $Ra = 3 \times 10^8$. The continuous line represents the best fit with a slope -0.54 ± 0.01.

dimensional prediction. The origin of this deviation is not known (and could originate from finite size effects of from the definition of the integral quantities entering in the dimensionless parameter), nonetheless it is worth remarking that a similar deviation has been found in numerical simulations of homogeneous convection forced by a mean temperature gradient [23].

3.2. 2D configuration

In 2D, in order to accurately describe the system statistics, we need to perform averages, to compute statistical observables, over several independent realizations (10 for each *Pr* value). This was not necessary in 3D as each realization is already averaged over the volume. In this case, the instability is induced by perturbing the interface with sinusoidal waves of small amplitude and different phase in each realization.

Figs. 3 and 4 summarize the results for *Nu* and *Re*, respectively, of the two-dimensional simulations. The main plots show the *Ra* dependence: our data follow the ultimate state predictions for $Ra > 5 \times 10^7$ and the agreement range spans three decades in the Rayleigh number.

In order to increase further the statistics, in the 2D case the *Pr* dependence is extracted as follows. Let us consider for example the Nusselt number. For each *Pr* value, let us suppose that we are able to identify a range of *Ra* values, $Ra_1 < Ra < Ra_2$, where

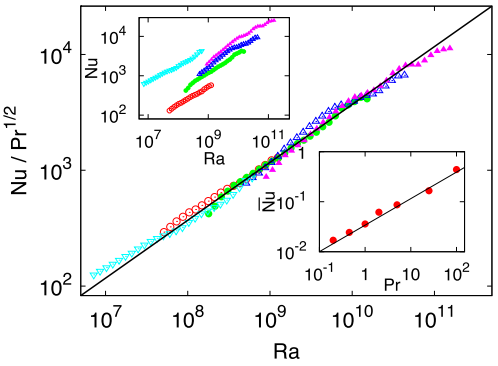

Fig. 3. *Nu* vs *Ra* obtained from 2D simulations at Prandtl numbers $Pr = 0.2$ (red, open circles), $Pr = 1.0$ (green, closed circles), $Pr = 2.0$ (blue, open upper triangles), $Pr = 5.0$ (pink, closed upper triangles), $Pr = 25$ (cyan, open lower triangles) (upper inset). Main plot: *Nu* compensated with the ultimate state prediction $Pr^{1/2}$ as a function of *Ra*. The line represents $Ra^{1/2}$. Lower inset: $\overline{Nu}$ vs *Pr* (see text for details). The line represents the best fit and the fitted slope is 0.53 ± 0.09.

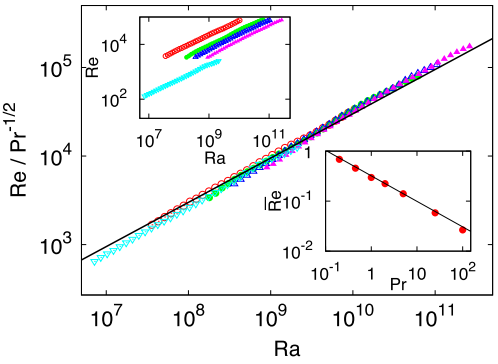

Fig. 4. *Re* vs *Ra* obtained from 2D simulations at different Prandtl numbers (colors and styles as in Fig. 3) (upper inset). Main plot: *Re* compensated with the ultimate state prediction $Pr^{-1/2}$ as a function of *Ra*. The line represents $Ra^{1/2}$. Lower plot: $\overline{Re}$ vs *Pr* (see text for details). The line is the best fit with a resulting slope of 0.51 ± 0.04.

$Nu(Ra, Pr)$ follows the dimensional prediction (6). On this range of *Ra* we compute the integral of the Nusselt number

$$\int_{Ra_1}^{Ra_2} Nu\, d(Ra) = C\, Pr^{1/2} \int_{Ra_1}^{Ra_2} Ra^{1/2}\, d(Ra), \tag{8}$$

where *C* is a numerical coefficient. To extract the dependence on *Pr* we define the average Nusselt number

$$\overline{Nu} \equiv \frac{\int_{Ra_1}^{Ra_2} Nu\, d(Ra)}{\frac{3}{2}\left(Ra_2^{3/2} - Ra_1^{3/2}\right)} \tag{9}$$

as a function of *Pr*.

The resulting average numbers for the 2D simulations are shown in the lower insets of Figs. 3 and 4. The best fit power laws give $Nu \sim Pr^{0.53 \pm 0.09}$ and $Re \sim Pr^{0.51 \pm 0.04}$, which are consistent with the ultimate state predictions (6)–(7).

4. Discussion and conclusions

Let us conclude by focusing our attention on the asymptotic limit $Pr \to \infty$. For a finite large value of *Pr*, provided that the time *t* is sufficiently small, the system undergoes a weakly nonlinear dynamics characterized by the balance between buoyancy and drag force. This latter regime has been the subject of much attention both theoretically [26–31], numerically [27,29,31] and experimentally [26].

The key point characterizing the weakly nonlinear phase is that the perturbation amplitude behaves linearly in time while the

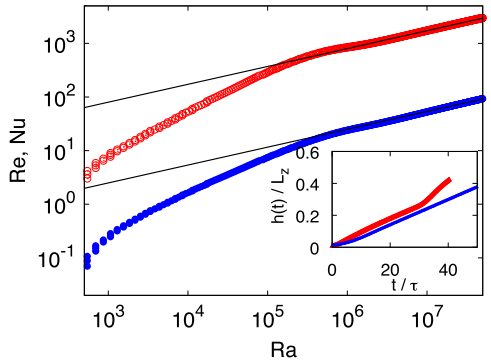

Fig. 5. *Nu* (upper, open red circles) and *Re* (lower, closed blue circles) as a function of *Ra* obtained from 2D simulations at $Pr = 100$ at short times. The two black lines represent the $Ra^{1/3}$ behavior. Inset: time evolution of amplitude perturbation $h(t)$ for two different Prandtl numbers: $Pr = 5$ (upper red points) and $Pr = 100$ (lower green points). Initial disturbances on mode $k = 9$ for $Pr = 5$ and $k = 3$ for $Pr = 100$. $\tau = (Agk)^{-1/2}$ is the linear growth time.

root-mean-square velocity is constant. As a consequence, Reynolds number *Re* grows as t and, as clear from simple dimensional considerations, the Nusselt number goes as $Nu \sim t$ and the Rayleigh number $Ra \sim t^3$. For finite large values of ν and sufficiently small times, the scaling of bulk quantities are:

$$Nu \sim Ra^{1/3}, \qquad Re \sim Ra^{1/3}. \tag{10}$$

As the *Pr* increases the time t at which the transition from the aforementioned weakly nonlinear phase and the fully developed turbulent regime also increases. In the asymptotic case (ideally $Pr \to \infty$) one expects that the duration of the weakly nonlinear phase characterized by the scaling law (10) diverges in time.

In Fig. 5 we show the behavior of *Nu* and *Re* as a function of *Ra* for $Pr = 100$. Continuous lines refer to the scaling expressed by (10). The inset shows that the duration of the weakly nonlinear phase increases by increasing *Pr*.

In conclusion, we report further evidences that Rayleigh–Taylor turbulence provides a natural laboratory for the emergence of the ultimate state regime of thermal convection. Moreover, we give evidences for a new scaling regime which clearly appears in the asymptotic limit $Pr \to \infty$.

References

[1] F. Cattaneo, T. Emonet, N. Weiss, On the interaction between convection and magnetic fields, Astrophys. J. 588 (2003) 1183.
[2] D.L. Hartmann, L.A. Moy, Q. Fu, Tropical convection and the energy balance at the top of the atmosphere, J. Clim. 14 (2001) 4495.
[3] E. van Doorne, B. Dhruva, K.R. Sreenivasan, V. Cassella, Statistics of wind direction and its increments, Phys. Fluids 12 (2000) 1529.
[4] S. Rashmostorf, The thermohaline ocean circulation – a system with dangerous thresholds? Clim. Change 46 (2000) 247.
[5] F.J. Marshall, F. Schott, Open-ocean convection: observations, theory, and models, Rev. Geophys. 37 (1999) 1.
[6] E. Siggia, High Rayleigh number convection, Annu. Rev. Fluid Mech. 26 (1) (1994) 137–168.
[7] D. Schultz, et al., The mysteries of Mammatus clouds: observations and formation mechanisms, J. Atmospheric Sci. 63 (2006) 2409–2435.
[8] W. Cabot, A. Cook, Reynolds number effects on Rayleigh–Taylor instability with possible implications for type Ia supernovae, Nat. Phys. 2 (8) (2006) 562.
[9] S. Fujioka, et al., Suppression of the Rayleigh–Taylor instability due to self-radiation in a multiablation target, Phys. Rev. Lett. 92 (19) (2004) 195001.
[10] J. Niemela, L. Skrbek, K. Sreenivasan, R. Donnelly, Turbulent convection at very high Rayleigh numbers, Nature 404 (2000) 837–840.
[11] D. Funfschilling, E. Bodenschatz, G. Ahlers, Search for the ultimate state in turbulent Rayleigh–Bénard convection, Phys. Rev. Lett. 103 (1) (2009) 014503.
[12] R. Stevens, R. Verzicco, D. Lohse, Radial boundary layer structure and Nusselt number in Rayleigh–Bénard convection, J. Fluid Mech. 643 (2010) 495–507.
[13] S. Grossmann, D. Lohse, Scaling in thermal convection: a unifying theory, J. Fluid Mech. 407 (2000) 27–56.
[14] G. Ahlers, S. Grossmann, D. Lohse, Heat transfer and large scale dynamics in turbulent Rayleigh–Bénard convection, Rev. Modern Phys. 81 (2) (2009) 503–537.
[15] R.H. Kraichnan, Turbulent thermal convection at arbitrary Prandtl number, Phys. Fluids 5 (11) (1962) 1374–1389.
[16] E. Spiegel, Convection in stars I. Basic Boussinesq convection, Ann. Rev. Astron. Astr. 9 (1) (1971) 323–352.
[17] M. Gibert, H. Pabiou, F. Chillà, B. Castaing, High-Rayleigh-number convection in a vertical channel, Phys. Rev. Lett. 96 (2006) 084501.
[18] M.R. Cholemari, J.H. Arakeri, Axially homogeneous, zero mean flow buoyancy-driven turbulence in a vertical pipe, J. Fluid Mech. 621 (2009) 69–102.
[19] A. Celani, A. Mazzino, L. Vozella, Rayleigh–Taylor turbulence in two dimensions, Phys. Rev. Lett. 96 (13) (2006) 134504.
[20] G. Boffetta, A. Mazzino, S. Musacchio, L. Vozella, Kolmogorov scaling and intermittency in Rayleigh–Taylor turbulence, Phys. Rev. E 79 (6) (2009) 065301.
[21] G. Boffetta, F. De Lillo, S. Musacchio, Nonlinear diffusion model for Rayleigh–Taylor mixing, Phys. Rev. Lett. 104 (3) (2010) 034505.
[22] D. Lohse, F. Toschi, Ultimate state of thermal convection, Phys. Rev. Lett. 90 (3) (2003) 034502.
[23] E. Calzavarini, D. Lohse, F. Toschi, R. Tripiccione, Rayleigh and Prandtl number scaling in the bulk of Rayleigh–Bénard turbulence, Phys. Fluids 17 (2005) 055107.
[24] D.H. Sharp, An overview of Rayleigh–Taylor instability, Physica D 12 (1984) 3–18.
[25] T. Matsumoto, Anomalous scaling of three-dimensional Rayleigh–Taylor turbulence, Phys. Rev. E 79 (5) (2009) 055301.
[26] J.T. Waddell, C.E. Niederhaus, J.W. Jacobs, Experimental study of Rayleigh–Taylor instability: Low Atwood number liquid systems with single-mode initial perturbations, Phys. Fluids 13 (5) (2001) 1263.
[27] V.N. Goncharov, Analytical model of nonlinear, single-mode, classical Rayleigh–Taylor instability at arbitrary Atwood numbers, Phys. Rev. Lett. 88 (13) (2003) 1345021.
[28] D. Layzer, On the instability of superposed fluids in gravitational field, Astrophys. J. 122 (1955) 1.
[29] U. Alon, J. Hecht, D. Ofer, D. Shvarts, Power laws and similarity of Rayleigh–Taylor and Richtmyer–Meshkov mixing fronts at all density ratio, Phys. Rev. Lett. 74 (4) (1995) 534.
[30] K.O. Mikaelian, Analytical approach to nonlinear Rayleigh–Taylor and Richtmyer–Meshkov instabilities, Phys. Rev. Lett. 80 (3) (1998) 508.
[31] Y.-N. Young, F.E. Ham, Surface tension in incompressible Rayleigh–Taylor mixing flow, J. Turbul. 7 (71) (2006) 1.